Pinning by an antidot lattice: The problem of the optimum antidot size

V. V. Moshchalkov, M. Baert, V. V. Metlushko,* E. Rosseel, M. J. Van Bael, K. Temst, and Y. Bruynseraede
Laboratorium voor Vaste-Stoffysica en Magnetisme, Katholieke Universiteit Leuven, B-3001 Leuven, Belgium

R. Jonckheere
Interuniversity Micro-Electronics Center, Kapeldreef 75, B-3001 Leuven, Belgium

(Received 19 February 1997; revised manuscript received 19 May 1997)

Critical current densities (j_c) and pinning forces (f_p) in superconducting Pb/Ge multilayers and single WGe films are strongly enhanced by introducing regular arrays of submicron holes (''antidot lattices'') acting as artificial pinning centers. Comparative measurements of j_c and f_p for several well-defined antidot diameters D have shown that pinning centers with a size considerably larger than the temperature-dependent coherence length $\xi(T)$ are much more efficient than those with a size close to $\xi(T)$. Moreover, the antidot size realizing the optimum pinning is field-dependent: we need smaller antidots to optimize pinning in lower fields and larger antidots for optimum pinning in higher fields. Crossover between different pinning regimes is controlled by the saturation number n_s that defines the largest possible number of flux lines trapped by an antidot. In dependence upon the n_s value, we have observed various composite flux lattices with vortices at antidots and interstices ($n_s \approx 1$), multiquanta vortex lattices ($n_s > 1$), and finally we have reached the limit of superconducting networks at $n_s \gg 1$. [S0163-1829(98)00906-0]

I. INTRODUCTION

The classical theory of the mixed state in homogeneous type-II superconductors[1] predicts the existence of the flux-line (FL) lattice. Each FL is carrying one flux quantum ϕ_0 and is characterized by the presence of a normal core with a size given by the temperature-dependent coherence length $\xi(T)$. In an ideal homogeneous superconductor without any defects, however, the Abrikosov FL lattice is not pinned and as a result the critical current density j_c tends to zero. Therefore the j_c enhancement, crucial for practical applications of superconducting materials, is closely related to the optimization of the size and the distribution of artificial pinning centers (the ''optimum pinning'' problem).

This problem can be successfully solved if both the *size* and the *pattern* of the introduced pinning centers are optimized. Since in a *homogeneous* superconductor the lowest energy FL configuration (triangular lattice) and the best size of the pinning centers [diameter $D \approx \xi(T)$] are known, it is widely believed that the triangular lattice of pinning centers with a size $\xi(T)$ is the best artificial pinning array.

This rather straightforward extrapolation of the results obtained for a *homogeneous* superconductor without pinning centers onto a superconductor *with artificial pinning centers* meets with serious controversies, since in many cases the presence of relatively large pinning centers also leads to a strong pinning. A quite instructive example here is the strongly enhanced pinning in the Y-Ba-Cu-O systems with precipitates such as CuO, Y_2BaCuO_5, or Y_2O_3, (Refs. 2–7) that have a size much larger than $\xi(T)$. To explain the efficiency of these relatively large precipitates, Takezawa and Fukushima have examined theoretically the behavior of a single insulating inclusion as a pinning center.[8] They have demonstrated that due to the electromagnetic contribution to pinning, the total pinning potential U, combining both electromagnetic U_B and core U_ψ contributions, is much deeper for $D \approx \lambda(T)$ than for $D \approx \xi(T)$. In other words, according to this theory, the optimum size of the insulating inclusion should be around the penetration depth $\lambda(T)$ rather than $\xi(T)$. This very interesting theoretical prediction has not been checked yet experimentally, since the previous studies were mainly focused on irradiation induced pinning centers[9,10] with a size and distribution that cannot be controlled properly. Following the pioneering work by Hebard and co-workers,[11] we have shown recently that *lithographically introduced submicrometer sized holes (antidots)* with a well-defined size and arranged in a regular pattern can act as efficient pinning centers.[12–15] Each antidot can trap up to n_s FLs, where n_s is a saturation number[16] $n_s \approx r_h/[2\xi(T)]$ and $2r_h = D$.

Using superconducting Pb/Ge and single WGe thin films with well-defined arrays of pinning centers, we have studied in this paper critical current densities j_c and pinning forces f_p for antidots with different diameters ($D = 0.15$ to 0.6 μm). The antidot arrays were introduced in the form of square or triangular lattices with a period $d = 1$ μm. From the *size dependence* of j_c and f_p we have confirmed that indeed pinning centers with *a size considerably larger than $\xi(T)$ are much more efficient than those with $D \approx \xi(T)$.* From the comparison of j_c and f_p in films with triangular and square lattices of antidots with the same D, we have found that in the former j_c and f_p are not very much higher than in the latter, which implies that the imposed artificial pinning potential is so strong that in this case the difference between the elastic energies of triangular and square lattice plays only a minor role. From detailed measurements of magnetization hysteresis loops $M(H,T)$ at different temperatures, we have found that the qualitative transformation of the $M(H,T)$ loops, caused by the variation of the antidot diameter D can also be induced by changing temperature T. In this way we have demonstrated that the pinning properties of an antidot lattice are fully controlled by the dimensionless parameter $D/\xi(T)$,

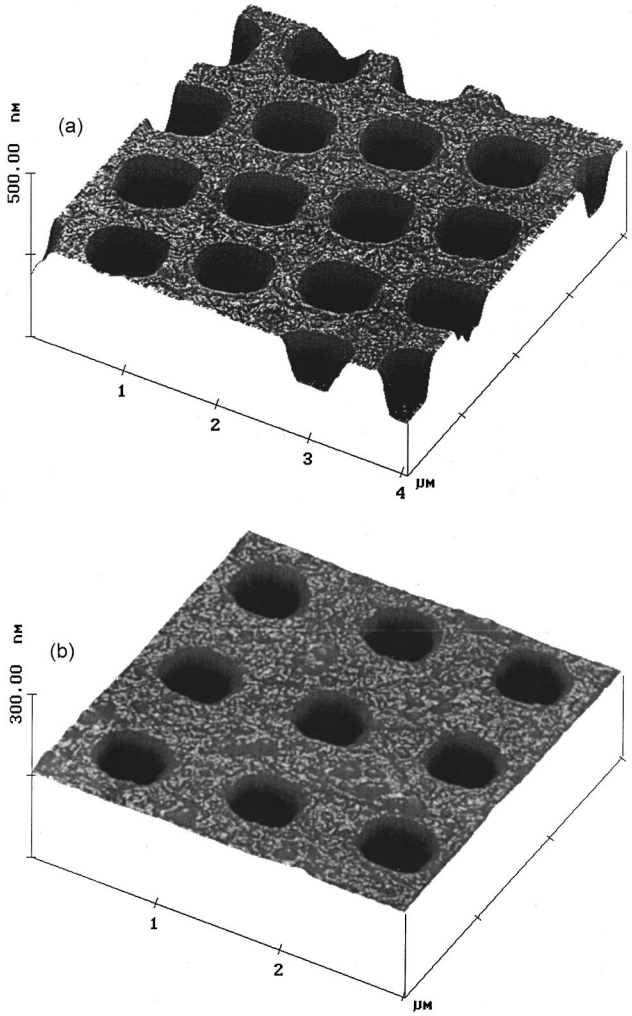

FIG. 1. (a) AFM picture of a $[\mathrm{Pb}(150\ \text{Å})/\mathrm{Ge}(140\ \text{Å})]_3$ multilayer with a square ''antidot'' lattice clearly shows the periodicity of the lattice $d=1\ \mu$m and the shape of the antidots with diameter $D=0.6\ \mu$m. (b) AFM picture of a single WGe(600 Å) film with a square ''antidot'' lattice ($d=1\ \mu$m and $D=0.35\ \mu$m).

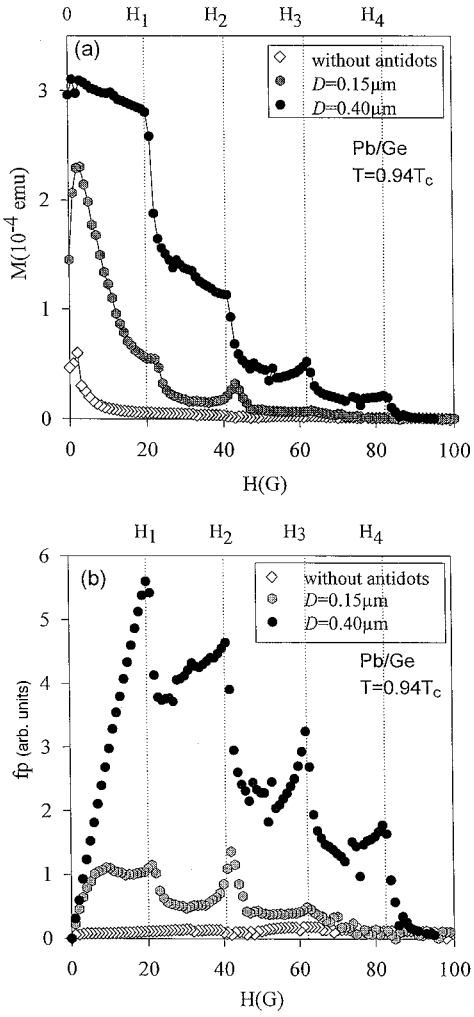

FIG. 2. (a) The magnetization curves ($T\approx 0.94\ T_C$) of the $[\mathrm{Pb}(150\ \text{Å})/\mathrm{Ge}(140\ \text{Å})]_3$ multilayer with a square lattice of antidots with diameter $D=0.15-0.4\ \mu$m. For comparison, the data for the reference multilayers without antidots are also shown. The matching fields $H_m\approx m$ 20.7 G (where m is an integer) are indicated by dashed lines. (b) The pinning force ($T\approx 0.94\ T_C$) of the $[\mathrm{Pb}(150\ \text{Å})/\mathrm{Ge}(140\ \text{Å})]_3$ multilayer with a square ''antidot'' lattice ($D=0.15-0.4\ \mu$m). For comparison, the data for the reference multilayers without antidots are also shown. The matching fields H_m are indicated by dashed lines.

in agreement with the theoretical prediction of Mkrtchyan and Shmidt[16] for a single antidot interacting with the FLs.

II. EXPERIMENT

The Pb/Ge multilayers and WGe single films are prepared by electron-beam evaporation in a molecular-beam epitaxy apparatus with a base pressure of 2×10^{-9} Torr. A detailed description of the sample preparation can be found in Ref. 17. All Pb/Ge samples have a $[\mathrm{Pb}(150\ \text{Å})/\mathrm{Ge}(140\ \text{Å})]_3\mathrm{Ge}$ structure, where 3 denotes the number of bilayers and the top film is always a 140 Å-thick protective Ge layer. The superconducting transition temperature of the Pb/Ge multilayers is $T_c=6.9$ K. The amorphous $W_{1-x}Ge_x$ ($x=0.33$) single films, with a thickness of 600 Å, were obtained by electron-beam evaporation of W and Ge, with $T_c=4.6$ K. The square or triangular lattices of antidots in the films were obtained by a lift-off technique using electron-beam lithography.

Figure 1(a) shows an atomic force microscopy (AFM) picture of a Pb/Ge multilayer with a square ''antidot'' lattice. The distance between the antidots is 1 μm and the surface between them is quite flat, the root-mean-square roughness is 1.5 nm on a $(0.5\ \mu\mathrm{m})^2$ area. An AFM picture of a WGe(600 Å) film with a square lattice of 0.35 μm antidots is shown in Fig. 1(b).

For our Pb/Ge multilayers, $\lambda(0)$ and $\xi(0)$ can be found using the dirty limit expressions $\xi(0)=(\xi_0 l)^{1/2}$ and $\lambda(0)=\lambda_0(\xi_0/l)^{1/2}$, where $\xi_0=83$ nm and $\lambda_0=37$ nm are the clean limit coherence length and penetration depth of Pb.[18] From the measured perpendicular upper critical field $H_{c2}(0)$ of the reference nonperforated films, we find that $\xi(0)=12$ nm and therefore $l\approx 17$ Å, $\lambda(0)\approx 260$ nm and the Ginzburg-Landau parameter $\kappa=21$. For the WGe(600 Å) single films we obtain the following values: $\xi(0)=6$ nm, $\lambda(0)=490$ nm, and $\kappa=82$.

Figure 2 shows the superconducting quantum interference device magnetization data for Pb/Ge multilayers without and

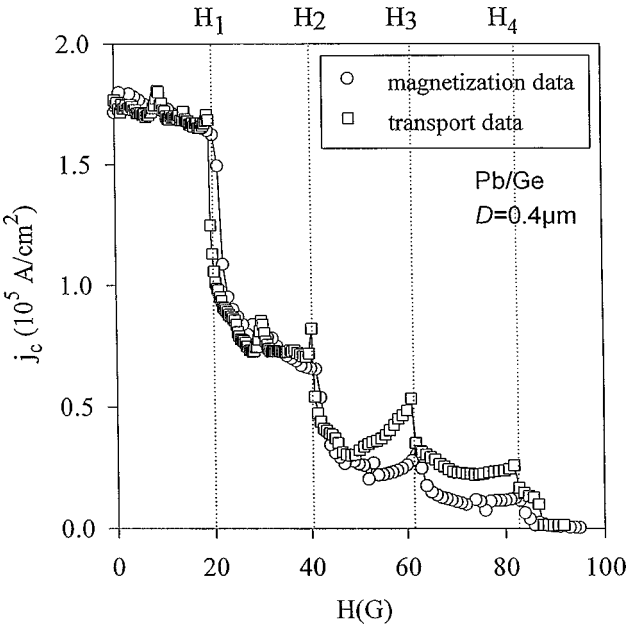

FIG. 3. Magnetic and transport critical current densities $j_c(H)$ for the [Pb(150 Å)/Ge(140 Å)]$_3$ multilayer with a square ''antidot'' lattice ($D=0.40\ \mu$m) at $T\approx 0.94\ T_C$.

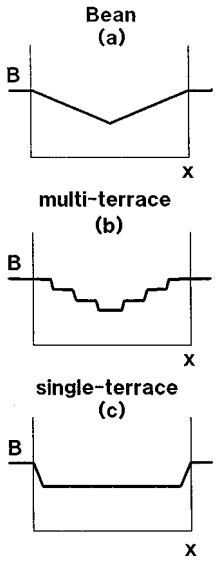

FIG. 4. Schematic drawing of the magnetic induction profile $B(x)$ for (a) classical Bean critical state, (b) multiterraced critical state (Ref. 20) and (c) single-terrace critical state.

with square antidot lattices ($D=0.15$ and $0.4\ \mu$m). The magnetization curves for multilayers with an antidot lattice clearly demonstrate sharp matching anomalies at the expected integer matching fields $H_m=m\phi_0/d^2$, where m is integer. For a square lattice with $d=1\ \mu$m, the H_m values are given by $H_m=m\times 20.7$ G. The matching anomalies, observed very clearly at temperatures not far below T_c, are related to stabilized ''flux-line crystals'', consisting of a square lattice of single or multiple flux quanta trapped by antidots. The origin of the sharp $M(H)$ features at $H=H_m$ has been discussed in our previous publications,[12–15] while here we would like to emphasize the overall enhancement of the width ΔM of the hysteresis loops, being compared with ΔM of the Pb/Ge multilayer without antidots.

Using the Bean model, modified for thin films in a perpendicular field,[19] we have estimated $j_c(H)$ from $\Delta M(H)$ and compared it with $j_c(H)$ determined from transport dc data (Fig. 3). This comparison shows a reasonably good agreement between j_c derived from ΔM and from transport measurements. Therefore, the anomalous variation of the width of the $M(H)$ loops is directly related to the change of $j_c(H)$. The latter is caused by a strong enhancement of the pinning force [Fig. 2(b)].

The $j_c(H)$ values, calculated in the framework of the classical Bean model,[19] should be considered only as an estimate, since in superconductors with the antidot lattices, instead of a smooth sandhill-like critical $B(x)$ profile [Fig. 4(a)], the novel multiterrace critical state should be introduced [Fig. 4(b)].[20] In the multiterrace critical state a competition between the vortex-antidot lattice commensurability and the average Bean-like gradient leads to the formation of the fluxon terraces. Within each terrace, the FL lattice is uniform and, therefore, there is no current, whereas at the terrace edges the critical current approaches its theoretical limit—the depairing current. The multiterrace critical state is, in a way, a quantized version of the classical Bean model. Since the average of the steplike $B(x)$ function corresponds to the Bean critical profile, the bean model still can be used to estimate the j_c value. Very close to T_c, where the expected average $B(x)$ slope is sufficiently small, the *single-terrace critical state* could be realized [Fig. 4(c)] with $B(x)$ being constant in the whole sample, except in the surface layer. As temperature goes down, the tendency towards the Bean critical state becomes stronger and the $B(x)$ terraces are eventually smeared out.[13]

Comparing now the $M(H)$ curves for $D=0.15\ \mu$m and $D=0.4\ \mu$m (Fig. 2), we clearly see that a much better pinning is provided by larger antidots [compare $M(H)$ and $f_p(H)$ curves for $D=0.15\ \mu$m and $D=0.4\ \mu$m]. For $D=0.4\ \mu$m, the field dependence of $j_c(H)$ becomes weaker and in low fields j_c values are smaller than for $D=0.15\ \mu$m. A very similar behavior with slightly higher $j_c(H)$ than for a square lattice has also been found for a triangular antidot lattice (Fig. 5), where matching anomalies are now observed at the expected field values $H_m=m2\phi_0/\sqrt{3}d^2=m23.9$ G. Analyzing $M(H)$ curves for different diameters ($D=0.17\ \mu$m and $D=0.4\ \mu$m) we find again that also for a triangular antidot lattice larger antidots [$D=0.4\ \mu\text{m}\gg\xi(T)$] are much more efficient for the enhancement of the pinning force.

Very similar magnetization data have also been obtained for a single WGe film with a square antidot lattice (Fig. 6) with different antidot diameters, from 0.15 to 0.6 μm. First of all, matching anomalies are again observed exactly at the expected matching fields $H_m=m20.7$ G. As the ratio $D/\xi(T)$ increases, the cusplike anomalies at matching fields are transformed into peaks (Fig. 7), typical for the superconducting networks. Second, in ''moderate'' magnetic fields $H<60$ G, we find the enhancement and then the reduction of the $M(H)$ values, as the antidot diameter is increased. However, in magnetic fields $H>60$ G, higher critical currents have been observed for the largest diameter of antidots (see Fig. 6, $D=0.6\ \mu$m), when the crossover to the superconducting network regime seems to occur. The latter implies that

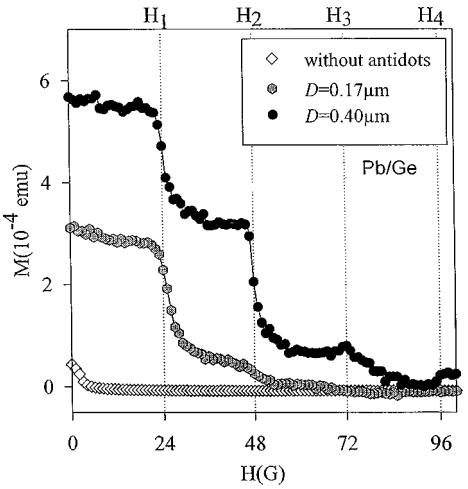

FIG. 5. The right upper parts of the magnetization curves ($T \approx 0.94\ T_C$) of the [Pb(150 Å)/Ge(140 Å)]$_3$ multilayer with a triangular ''antidot'' lattice ($D = 0.17-0.4\ \mu$m). The matching fields $H_m \approx m$ 23.9 G are indicated by dashed lines.

the optimum size of the antidots, realizing the best pinning, is field-dependent.

The comparison of the size dependence of $M(H)$ [Fig. 8(a)] with the temperature dependence of the $M(H)$ for the fixed $D = 0.5\ \mu$m [Fig. 8(b)], reveals an important similarity between the modification of the $M(H)$ behavior induced by the variation of the antidot diameter D and the temperature dependence $M(H,T)$ for the same $D = 0.15\ \mu$m.

This similarity indicates that the relevant parameter of the optimum pinning problem is the ratio $D/\xi(T)$, in agreement with the calculations of Shmidt and Mkrtchyan[16] of the pinning potential for flux lines interacting with a single antidot.

III. DISCUSSION

In this section we shall focus on the following points, which are quite important for our understanding of the optimum pinning problem: (i) general behavior of $M(H)$ curves, as a function of the antidot diameter, (ii) pinning of multiquanta vortex lattices, (iii) crossover from the periodic array of small pinning centers to the network array, when the width of the superconducting stripes becomes smaller than the coherence length $\xi(T)$.

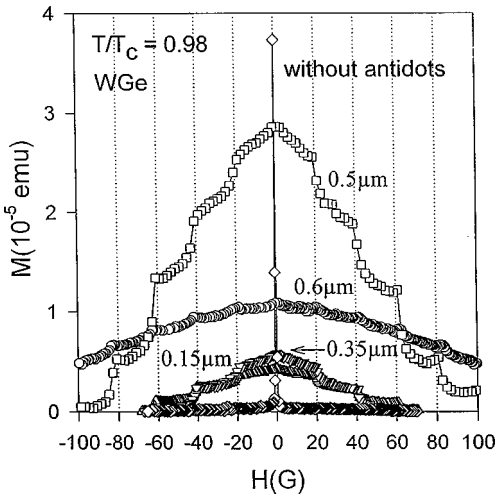

FIG. 6. The magnetization curves ($T = 0.98\ T_C$) of a single WGe(600 Å) film with a square lattice of antidots with diameter $D = 0.15-0.6\ \mu$m. For comparison, the data for the reference multilayers without antidots are also shown. The matching fields $H_m \approx m$ 20.7 G (where m is an integer) are indicated by dashed lines.

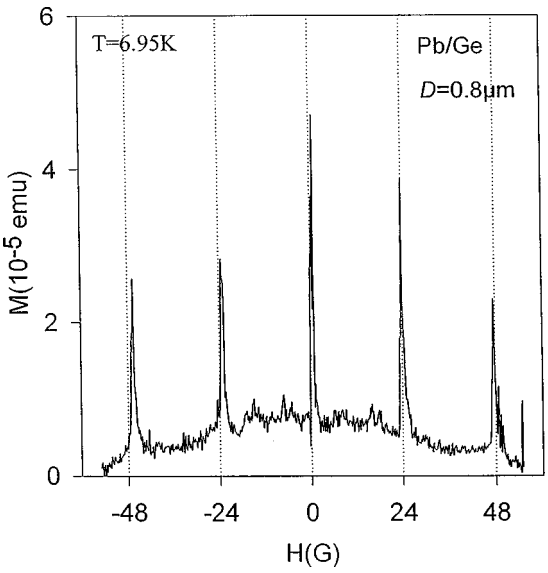

FIG. 7. The upper magnetization curve at $T = 6.95$ K of the [Pb(150 Å)/Ge(140 Å)]$_3$ multilayer with triangular antidot lattice ($D = 0.8\ \mu$m).

A. Magnetization curves for different antidot diameters

Our main experimental observations can be summarized as follows: (a) artificial arrays of submicron antidots can act as well-defined pinning centers with a controlled size and pattern; (b) distinct matching anomalies show up at the expected fields $H_m = m\phi_0/S$, where S is the unit cell of the antidot lattice; (c) increasing the antidot diameter, we have found a clear evidence of a stronger pinning by square and triangular arrays consisting of antidots larger than $\xi(T)$; and (d) similar size dependence of the pinning force is observed not only in Pb/Ge and WGe/Ge multilayers but also in single Pb and WGe films.

At the typical used reduced temperature $T/T_c = 0.94$ (Fig. 2), we have $\xi(T) \approx 0.1\ \mu$m. Therefore the size $D \approx 0.15\ \mu$m of the smaller antidots is quite close to $\xi(T)$ and should give us the optimum pinning, if the condition $\xi(T) \approx D$ is correct in our case and the core pinning potential U_p plays a dominant role. Since for larger antidots pinning has been further enhanced, we are sure that for antidots with $D \gg \xi(T)$ pinning is much stronger than that for $D \approx \xi(T)$. The latter confirms that electromagnetic pinning U_p indeed gives an important contribution: according to Ref. 8 the depth of U_p increases rapidly with D and saturates at $D \approx \lambda(T)$. Unfortunately, further quantitative comparison with the theory of Takezawa and Fukushima[8] is not possible, since they have calculated the pinning potential but not the pinning force and, second, they have considered the limit of a single pinning center, whereas in our case the circular currents around different antidots are overlapping: in our films $\Lambda = 2\lambda^2(T)/t > d$. Here t is the thickness of an individual Pb

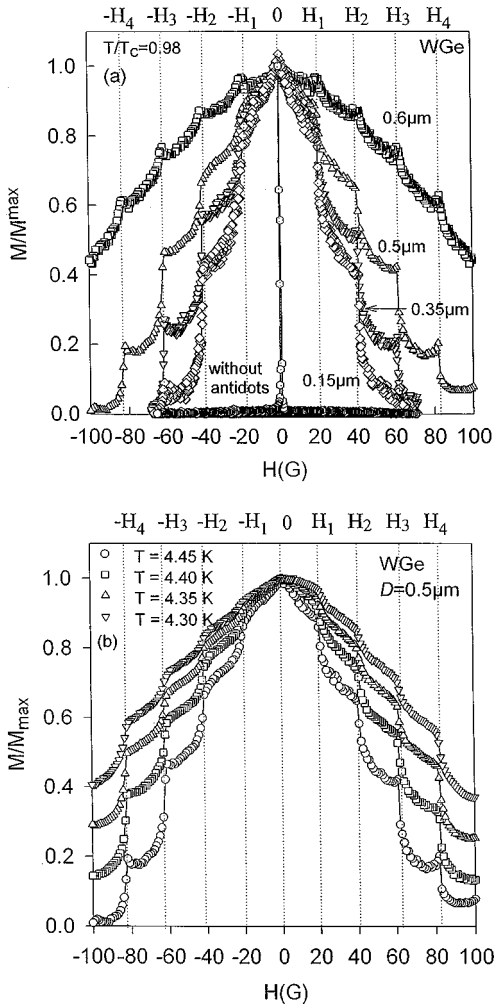

FIG. 8. (a) Normalized magnetization curves ($T=0.98\ T_C$) of a single WGe(600 Å) film with a square lattice of antidots with diameter $D=0.15-0.6\ \mu$m. For comparison, the data for the reference multilayers without antidots are also shown. The matching fields $H_m \approx m$ 20.7 G (where m is an integer) are indicated by dashed lines. (b) The magnetization curves at different temperatures of a single WGe(600 Å) film with a square lattice of antidots with diameter $D=0.5\ \mu$m. The matching fields $H_m \approx m$ 20.7 G (where m is an integer) are indicated by dashed lines.

layer or the whole multilayer for decoupled or coupled superconducting layers, respectively. In our films we have $\Lambda > d$, and for qualitative analysis of our data lattice effects should be taken into consideration in calculations of U_B, which has not been done in Ref. 8.

The sharp magnetization anomalies at the matching field were nicely reproduced in calculations of Cooley and Grishin,[20] who showed that the appearance of the terraced critical state [Fig. 4(b)] results in magnetization jumps with the periodicity corresponding to ϕ_0 per antidot lattice unit cell.

For small antidot radii ($n_s \approx 1$), a substantial reduction of j_c can occur when the antidots are saturated[21] and additional vortices are formed at interstices. In this case very weakly pinned interstitial vortices are much more mobile than the vortices pinned by the antidots.[22] As a result, the motion of interstitial vortices leads to a dissipation and j_c is reduced. The dynamics and plastic flow of vortices in superconductors with coexisting interstitial FLs and vortices pinned by antidots has been recently studied by Reichhardt *et al.* by numerical simulations.[23] Due to a higher mobility of interstitial vortices, larger antidots seem to be better since they can stabilize multiquanta vortices and there is no need to produce loosely bound interstitial vortices.

Concluding this section we have shown that *antidots with D considerably larger than the coherence length ξ(T) are efficient pinning centers*. This conclusion is valid for different superconductors we studied. As a possible explanation for the stronger pinning by larger antidots, we refer to the electromagnetic contribution to pinning, U_B, recently analyzed by Takezawa and Fukushima.[8]

B. Pinning of multiquanta vortex lattices

Sufficiently large antidots ($n_s \gg 1$) can pin multiquanta vortices.[24–26] In this case for temperatures very close to T_c, we have a possibility to realize the single-terrace critical state with $B(x)=$constant and the following expression can be used to analyze magnetization curves $M(H)$ (Ref. 26):

$$M(H) = -\frac{\phi_0}{16\pi^2\lambda^2}\ln\left(\frac{\beta a_\nu}{\sqrt{e}r}\right). \tag{1}$$

This expression is obtained by inserting the size of the core $\xi(T)\to r$, and the vortex-vortex distance a_ν into the textbook expression[18] for magnetization in the London limit. In Eq. (1) β is a numerical constant which is 0.381 for a triangular vortex lattice in nonperforated films.[18] When multiquanta vortices are formed (Fig. 5) Eq. (1) takes an extremely simple form exactly at the matching fields $H=H_m$ since $m\phi_0$ should then be used instead of ϕ_0 and a_ν is just the antidot lattice period d:

$$M(H_m) = -\frac{m\phi_0}{16\pi^2\lambda^2}\ln\left(\frac{\delta d}{\sqrt{e}r}\right) \propto \frac{m\phi_0}{\lambda^2}. \tag{2}$$

The magnetization at $H=H_m$ is a linear function of m, with the slope determined via prefactor $\sim 1/\lambda^2(T)$ in Eq. (2). For intermediate size of antidots ($D=0.5\ \mu$m) this dependence is clearly observed (see dashed lines in Fig. 9).

Between the matching fields $H_m<H<H_{m+1}$ the magnetization M can be approximated by[26]

$$M(H_m<H<H_{m+1}) \cong -\frac{\tilde{\phi}_{om}}{16\pi^2\lambda^2}\ln\left[\frac{\beta_{\rm eff}}{\sqrt{e}r}\left(\frac{\phi_0}{H\text{-}H_m}\right)^{1/2}\right], \tag{3}$$

which gives us another possibility to find $\lambda(T)$. Previously,[26] we have used Eq. (3) to determine the effective flux $\tilde{\phi}_{om}$ for different field intervals (H_m, H_{m+1}) keeping temperature constant. Here, in this paper, we fix the interval (H_m, H_{m+1}) but follow the modifications in the cusplike decrease of $M(H)$ as a function of temperature. The slope M vs $\ln(H\text{-}H_m) \propto 1/\lambda^2(T)$ indeed is changed as we expect from the growth of $\lambda(T)$ with increasing temperature [Fig. 10(a)]. The existence of multiquanta vortices, proposed from the analysis of the magnetization data, has been recently convincingly confirmed in magnetic decoration experiments.[25]

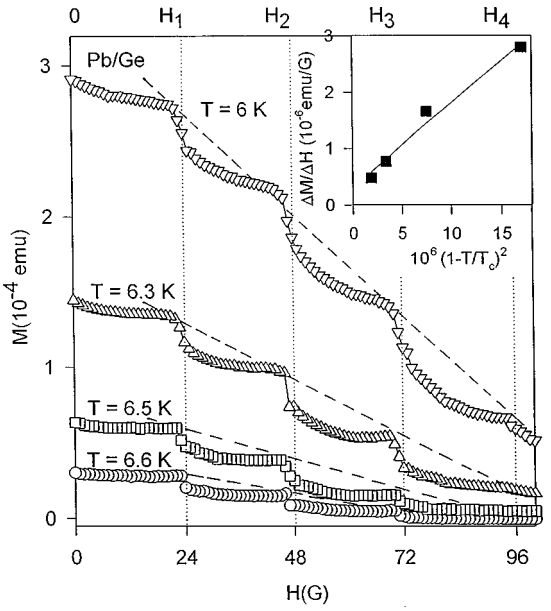

FIG. 9. The right upper parts of the magnetization loops $M(H)$ at different temperatures for the $[\mathrm{Pb}(100\ \text{Å})/\mathrm{Ge}(50\ \text{Å})]_2$ multilayer with an antidot lattice. The dashed lines, at different temperatures, clearly indicate the linear behavior of $M(H_m)$ as a function of the integer m. The insert presents the slopes $\Delta M/\Delta H$ of the dashed lines, as a function of $[1-(T/T_C)]^2$. According to Eq. (2) these slopes follow the temperature dependence of $1/\Lambda^2$. The solid line presents the linear fit.

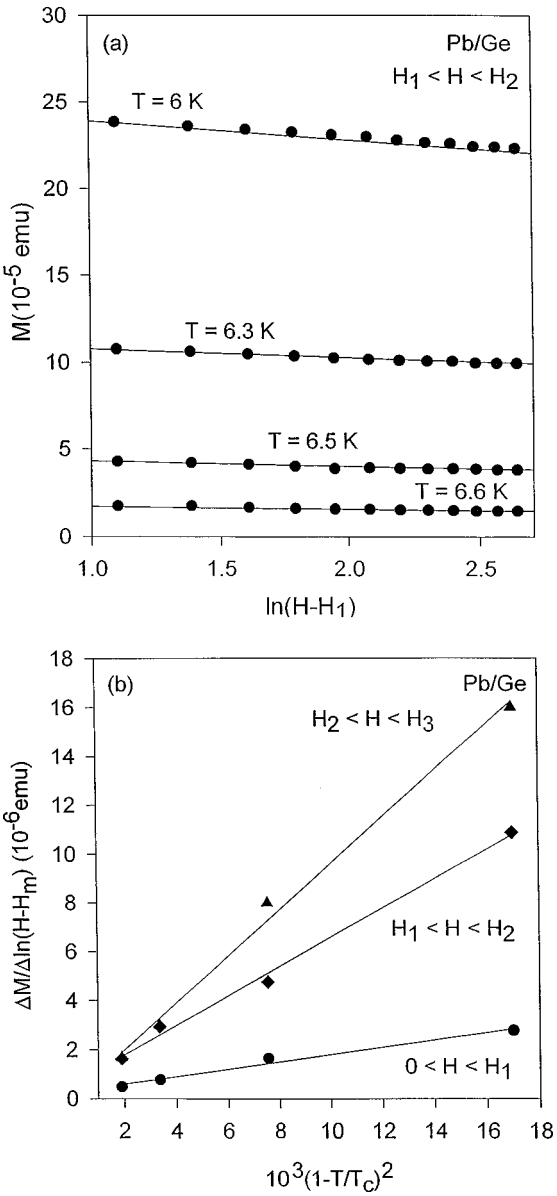

FIG. 10. (a) The magnetization M vs $\ln(H\text{-}H_1)$ at different temperatures for a $[\mathrm{Pb}(100\ \text{Å})/\mathrm{Ge}(50\ \text{Å})]_2$ multilayer with an antidot lattice. (b) The different slopes of the solid lines at different temperatures in Fig. 10(a) are plotted for the different periods. These slopes follow the temperature dependence of $1/\Lambda^2$.

At first sight, it might be considered as a surprise that Eqs. (2) and (3) for the interpretation, derived from the expressions for the three-dimensional (3D) superconductors, work quite well also for our films [see Figs. 9, 10(a), and 11(a)]. This apparent controversy is however resolved due to the two important reasons:

(i) In *multilayers*, contrary to a single film,[27] the interaction between the vortex lines, consisting of pancake vortices, is *logarithmic* to all distances.[28] This nicely corresponds to the logarithmic interaction in the 3D case on which Eqs. (2) and (3) are based.

(ii) In contrast with the singly connected films, we deal with *multiply connected perforated thin films*, where the in-plane distance between the antidots (about 0.5 μm) is comparable with the film thickness (about 0.1 μm). The ratio of this characteristic lateral dimension/thickness is only about 5, which is still in the 3D limit. This ratio is orders of magnitude smaller than 10^4-10^6 in nonperforated thin films, for which the vortex-vortex interactions are in the 2D regime. Since the flux lines penetrate through antidots, the relevant characteristic lateral size of the *perforated* films is the distance between the antidots and not the sample's full lateral dimensions.

An important remark should be made here concerning the irreversibility of the magnetization. We think that the irreversibility of the perforated superconducting film is mainly caused by its multiple connectivity (that is, by the way, also the case with the pinned vortex lattice in the framework of a conventional Bean model). The superconducting current flowing around antidots is similar to a circular supercurrent in a ring. As it was already emphasized by Schoenberg quite some time ago (see, for example, Ref. 29 and references therein) a ring, as a multiply connected body, demonstrates a strong irreversible response. Along similar lines, the calculations of Cooley and Grishin[20] are also reproducing the magnetization irreversibility in a multiply connected superconductor with an antidot lattice.

The next important problem to discuss is which λ to take in the expressions (1)–(3), if to use it for films with antidot lattices. The answer for nonperforated films is well known: due to the renormalization of the penetration depth (Ref. 18) $\lambda(T)$ should be replaced by $\Lambda=2\lambda^2(T)/t$, with t the thickness of the film. Keeping two possible options in mind: $1/\lambda^2(T)$ or $1/\Lambda^2(T)$ for the prefactor in Eq. (3), we have plotted the slopes of the dashed lines in Fig. 9 [see also Eq. (2)] and solid lines between matching fields $H_m<H<H_{m+1}$ [Eq. (3)] both vs $(1-T/T_c)$ and $(1-T/T_c)^2$, as it can be anticipated from $1/\lambda^2(T)$ and $1/\Lambda^2(T)$, respectively.

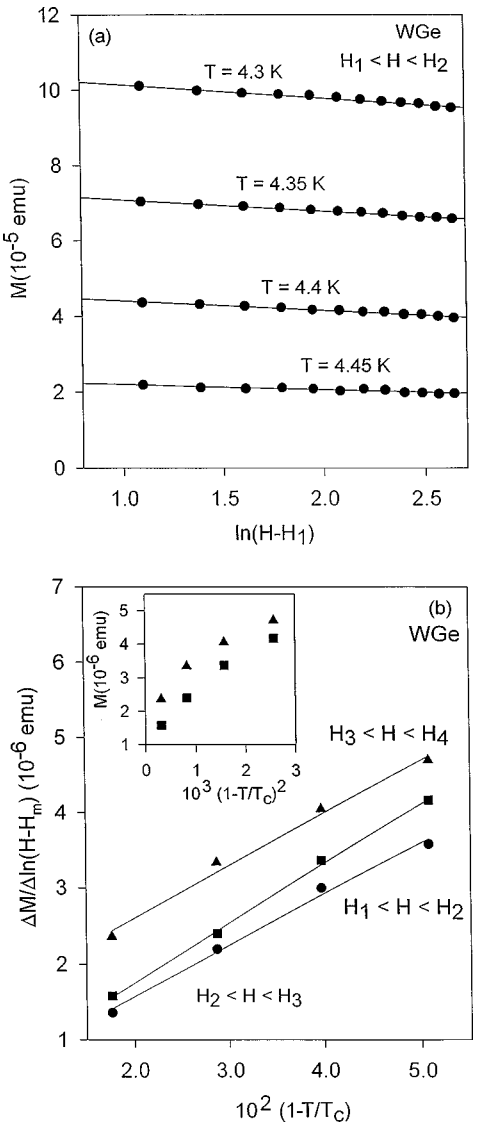

FIG. 11. (a) The magnetization M vs $\ln(H\text{-}H_1)$ at different temperatures for a WGe(600 Å) single film with an antidot lattice. (b) The different slopes of the solid lines at different temperatures in (a) are plotted for the different periods. These slopes follow the temperature dependence of $1/\lambda^2$, better than the dependence expected from $1/\Lambda^2$ (see the insert).

For the Pb/Ge multilayers the best linearity is obtained for the $\Delta M/\Delta\ln(H\text{-}H_m)$ vs $(1-T/T_c)^2$ plots [see Fig. 10(b)]. For the WGe single films (Fig. 11) it is clearly seen from Fig. 11(b), that a better linearity is always obtained for the plots $\Delta M/\Delta\ln(H\text{-}H_m)$ vs $1-T/T_c$, i.e., ''normal'' $\lambda(T)$ should be used in perforated superconducting films with an antidot lattice. We can interpret this observation as a consequence of a much easier flux-line penetration through the antidots in a perforated film with respect to a reference film, where $\Lambda(T)$ should be used. Moreover, the total area of the antidots S_a is to be subtracted from the total sample area S_s when considering flux penetration into a film with antidots. As a result $\lambda(T)$ should be renormalized as follows:[30] $1/\lambda^2(T)\rightarrow 1/\lambda^2(T)(1-2S_a/S_s)$. The factor 2 in this expression is obtained from calculations in the London limit. Without this factor the $\lambda(T)$ renormalization is just the result of taking into account the area of the antidots.

C. Crossover from a pinning array to a network

The systematic measurements of the efficiency of antidots, as artificial pinning centers, as a function of their diameter D (Fig. 6) have revealed that for core pinning combined with the electromagnetic pinning the optimum size of the antidots is not $\xi(T)$ at all, but rather $D\gg\xi(T)$. As a result, we have obtained the highest critical currents for the multiquanta vortex lattices that can be stabilized by these sufficiently large antidots, since their saturation number is $n_s\sim D/\xi(T)\gg 1$. At the same time it is quite evident that by increasing the antidot diameter we are inducing a crossover to another regime (Fig. 7) when eventually D becomes nearly the same as the antidot lattice period d. In this case the width of the superconducting stripes w_s between the antidots is so small that at temperatures not too far below T_c the superconducting network regime $w_s\leqslant\xi(T)$ can be realized. For this regime the M vs H curves are characterized by the presence of sharp peaklike anomalies at integer matching fields H_m (Fig. 7) and a reproducible structure between H_m, which may correspond to rational matching peaks. Both integer and rational matching peaks have been observed before in various superconducting networks[31] and Josephson networks.[32] Visually the $M(H)$ curves in the *network* regime are quite different from those in the *multiquanta* vortex regime: the former demonstrate the $M(H)$ *peaks* at $H=H_m$ (Fig. 7), while the latter show pronounced *cusps* at integer fields [Fig. 8(b)].

In the regime of a superconducting network, critical currents in moderate fields are already smaller than for the regime of the multiquanta vortex lattices (see Fig. 6). At higher fields, however, at least for the diameter $D=0.6\ \mu$m, critical currents are better for the largest studied antidot diameter, i.e., the optimum antidot size is field-dependent. The reduction of the width of the superconducting ''stripes'' between the antidots, needed to obtain high j_c in high fields, reflects actually a well-known designer rule for making superconducting cables, which usually consist of a bunch of very fine superconducting filaments embedded into a normal metallic matrix.

IV. CONCLUSIONS

We have performed a systematic study of the critical current enhancement due to the presence of the antidots, used as artificial pinning arrays. Different regimes can be clearly distinguished in dependence upon the antidot diameter. For *small antidots* with the saturation number $n_s=1$ the existence of the *two types of vortices* (weakly pinned at interstices and strongly pinned at antidots) should be taken into account.[15,21,22] The motion of the interstitial vortices gives rise to a dissipation and therefore further j_c enhancement can be provided by taking larger antidots. For these antidots the saturation number n_s becomes sufficiently large ($n_s\gg 1$) to stabilize the *multiquanta vortex lattices*. We are able to obtain the highest enhancement factor for j_c in moderate fields. The size of the antidots in this case is considerably larger than $\xi(T)$ and therefore an electromagnetic contribution to pinning plays also an important role. For multiquanta vortex lattices we have proposed a simple approach, developed in the framework of the London limit, which gives an excellent fit of the experimental $M(H,T)$ curves for different tempera-

tures. This implies that by making antidot lattices we can substantially expand the area on the H-T plane where the London limit is still valid. In the same framework, the variation of such a fundamental parameter as $\lambda(T)$ can be achieved just by taking different antidot radii. The renormalization of $\lambda(T)$ (Ref. 30) is directly related to a different topology of films with an antidot lattice that make the flux-line penetration much easier.

By a further increase of the antidot diameter we have induced a crossover to the regime of *superconducting networks* with sharp $M(H)$ peaks at integer fields H_m, in contrast with the $M(H)$ cusps at H_m in case of multiquanta vortex lattices.

Finally, since the saturation number n_s, controlling the onset of different regimes (small n_s: composite flux lattices with vortices at antidots and interstices; large n_s: multiquanta vortex lattices; very large n_s: superconducting networks) is determined by the ratio $r/2\xi(T)$, the n_s value can be tuned not only by taking different antidot radii, but also by varying temperature and $\xi(T)$.

ACKNOWLEDGMENTS

This work was supported by the Belgian Interuniversity Attraction Poles (IUAP), Flemish Concerted Action Programs (GOA), International Association for the promotion of cooperation with scientists from the independent states of the former Soviet Union (INTAS), and by the Fund for Scientific Research (FWO-Vlaanderen). We would like also to acknowledge useful discussions with C. Van Haesendonck. M. Baert is supported by the Research Council of the K. U. Leuven. E. Rosseel is supported by the Belgian Interuniversity Institute for Nuclear Sciences (I.I.K.W.) while M.J.V.B. is supported by the Fund for Scientific Research (FWO).

*Present address: Materials Science Division, Argonne National Laboratory, 9700 South Cass Avenue, MSD/223, Argonne, IL 60439-4845.

[1] A. A. Abrikosov, Zh. Eksp. Teor, Fiz. **32**, 1442 (1957) [Sov. Phys. JETP **5**, 1174 (1957)].

[2] M. Murakami, M. Morita, K. Doi, and K. Miyamoto, Jpn. J. Appl. Phys., Part 1 **28**, 1189 (1989).

[3] K. Yamaguchi, M. Murakami, H. Fujimoto, S. Gotoh, N. Koshizuka, and S. Tanaka, Jpn. J. Appl. Phys., Part 2 **29**, L1428 (1990).

[4] S. Matsuno, S. Kinouchi, K. Egawa, T. Umemura, F. Uchikawa, and S. Nakabayashi, Appl. Phys. Lett. **62**, 1556 (1993).

[5] P. J. Kung, M. P. Maley, M. E. McHenry, J. O. Willis, M. Murakami, and S. Tanaka, Phys. Rev. B **48**, 13 922 (1993).

[6] Y. Q. Li, J. Zhao, C. S. Chern, P. Lu, T. R. Chien, B. Gallois, P. Norris, B. Kear, and F. Cosandey, Appl. Phys. Lett. **60**, 2430 (1992).

[7] D. Shi, M. S. Boley, U. Welp, J. G. Chen, and Y. Liao, Phys. Rev. B **40**, 5255 (1989).

[8] N. Takezawa and K. Fukushima, Physica C **228**, 149 (1994).

[9] W. Gerhäuser, G. Ries, H. H. Neumüller, W. Schmidt, O. Eibl, G. Saeman-Ischenko, and S. Klaumünzer, Phys. Rev. Lett. **68**, 879 (1992).

[10] L. Civale, A. D. Marwick, T. K. Worthington, M. A. Kirk, J. R. Thompson, L. Krusin/Elbaum, Y. Sun, J. R. Clem, and F. Holtzberg, Phys. Rev. Lett. **67**, 648 (1991).

[11] A. F. Hebard, A. T. Fiory, and S. Somekh, IEEE Trans. Magn. **1**, 589 (1977).

[12] V. V. Metlushko, M. Baert, R. Jonckheere, V. V. Moshchalkov, and Y. Bruynseraede, Solid State Commun. **91**, 331 (1994).

[13] V. V. Moshchalkov, L. Gielen, M. Baert, V. Metlushko, G. Neuttiens, C. Strunk, V. Bruyndoncx, X. Qiu, M. Dhallé, K. Temst, C. D. Potter, R. Jonckheere, L. Stockman, M. Van Bael, C. Van Haesendonck, and Y. Bruynseraede, Phys. Scr. **I55**, 168 (1994).

[14] M. Baert, V. V. Metlushko, R. Jonckheere, V. V. Moshchalkov, and Y. Bruynseraede, Europhys. Lett. **29(2)**, 157 (1995).

[15] M. Baert, V. V. Metlushko, R. Jonckheere, V. V. Moshchalkov, and Y. Bruynseraede, Phys. Rev. Lett. **74**, 3269 (1995).

[16] G. S. Mkrtchyan and V. V. Shmidt, Zh. Eksp. Teor. Fiz. **61**, 367 (1971) [Sov. Phys. JETP **34**, 195 (1972)].

[17] Y. Bruynseraede, K. Temst, E. Osquiguil, C. Van Haesendonck, A. Gilabert, and I. K. Schuller, Phys. Scr. **42**, 37 (1992).

[18] P. G. de Gennes, *Superconductivity of metals and alloys* (Addison-Wesley, New York, 1966).

[19] C. P. Bean, Phys. Rev. Lett. **8**, 250 (1962); E. H. Brandt, Phys. Rev. B **50**, 4043 (1994); J. Wang and M. Sayer, Physica C **212**, 385 (1993); P. N. Mikheenko and Yu. E. Kuzovlev, *ibid.* **204**, 229 (1993).

[20] L. D. Cooley and A. M. Grishin, Phys. Rev. Lett. **74**, 2788 (1995).

[21] E. Rosseel, M. Van Bael, M. Baert, R. Jonckheere, V. V. Moshchalkov, and Y. Bruynseraede, Phys. Rev. B **53**, R2983 (1996).

[22] K. Harada, O. Kamimura, H. Kasai, T. Matsuda, A. Tonomura, and V. V. Moshchalkov, Science **274**, 1167 (1996).

[23] C. Reinhardt, J. Groth, C. J. Olson, S. B. Field, and F. Nori, Phys. Rev. B **54**, 16 108 (1996).

[24] A. I. Buzdin, Phys. Rev. B **47**, 11 416 (1993).

[25] A. Bezryadin and B. Pannetier, J. Low Temp. Phys. **102**, 73 (1996).

[26] V. V. Moshchalkov, M. Baert, V. Metlushko, E. Rosseel, M. Van Bael, K. Temst, R. Jonckheere, Y. Bruynseraede, Superlattices Microstruct. **19**, 3 (1996); Phys. Rev. B **54**, 7385 (1996).

[27] J. Pearl, Appl. Phys. Lett. **5**, 65 (1964).

[28] J. R. Clem, in *The Vortex State*, Vol. 438 of *NATO Aduanced Study Institute, Series C*, edited by N. Bontemps, Y. Bruynseraede, G. Deutscher, and A. Kapitulnik (Kluwer-Academic, New York, 1994).

[29] D. Schoenberg, *Superconductivity* (Cambridge University Press, Cambridge, England, 1965), p. 27.

[30] A. Buzdin and D. Feinberg, Physica C **256**, 303 (1996).

[31] B. Pannetier, J. Chaussy, R. Rammal, and J. C. Villegier, Phys. Rev. Lett. **53**, 1845 (1984).

[32] W. J. Elion, H. S. J. Van Der Zant, and J. E. Mooij, *Macroscopic Quantum Phenomena and Coherence in Superconducting Networks* (World Scientific, Singapore, 1995), p. 105.